PHYSICAL REVIEW B **90**, 054511 (2014)

Vortices and charge order in high-T_c superconductors

M. Einenkel,[1,2] H. Meier,[3] C. Pépin,[4] and K. B. Efetov[1,2]
[1]*Institut für Theoretische Physik III, Ruhr-Universität Bochum, 44780 Bochum, Germany*
[2]*National University of Science and Technology "MISiS," Moscow 119049, Russia*
[3]*Department of Physics, Yale University, New Haven, Connecticut 06520, USA*
[4]*IPhT, L'Orme des Merisiers, CEA-Saclay, 91191 Gif-sur-Yvette, France*
(Received 21 July 2014; published 19 August 2014)

We theoretically investigate the vortex state of the cuprate high-temperature superconductors in the presence of magnetic fields. Assuming the recently derived nonlinear σ-model for fluctuations in the pseudogap phase, we find that the vortex cores consist of two crossed regions of elliptic shape, in which a static charge order emerges. Charge density wave order manifests itself as satellites to the ordinary Bragg peaks directed along the axes of the reciprocal copper lattice. Quadrupole density wave (bond order) satellites, if seen, are predicted to be along the diagonals. The intensity of the satellites should grow linearly with the magnetic field, in agreement with the result of recent experiments.

DOI: 10.1103/PhysRevB.90.054511 PACS number(s): 74.40.Kb, 74.25.Ha, 74.25.Uv

I. INTRODUCTION

Since their discovery [1] in 1986, high-temperature (high-T_c) superconductors remain one of the most interesting fields of research in modern condensed-matter physics. In particular, the origin of the pseudogap (PG) phase, appearing below a temperature T^* of the order of a few 100 K, remains one of their most enduring mysteries. The field has revived recently through a number of spectacular experimental findings [2–10], which all give evidence to the presence of charge patterns inside the PG phase. Understanding the properties of these charge-ordered phases, competing or coexisting with superconductivity (SC), may significantly help to clarify the physical origin of the PG phase.

While a stripe order combining both charge and spin modulations first predicted theoretically in Refs. [11–13] has been known for a long time to exist in La compounds [14–17], the first observation of a modulated structure in $Bi_2Sr_2CaCu_2O_8$ (BSCCO) was reported only in 2002 by Hoffman *et al.* [18], who subtracted the scanning tunneling microscope (STM) response with and without an applied magnetic field and thus unearthed a checkerboard charge order inside the vortex cores. At the time, it was still interpreted in terms of the stripes similar to those La compounds. It was found that the radius of the region where this order appears is larger than the radius of the vortex cores. The close connection between the development of an ordered state and the formation of vortices due to an applied magnetic field has been confirmed by a number of experiments [19,20]. It has recently become clear that the high-T_c compounds of BSCCO and $YBa_2Cu_3O_{7-x}$ (YBCO) feature a checkerboard-type charge modulation with wave vectors along the bonds of the CuO lattice [4,6–10,21].

Further, it is well known that under application of a strong magnetic field exceeding 17 T, a striking reconfiguration of the Fermi surface is observed [22,23]. After an intense debate, a consensus emerged in which the reconfiguration of the Fermi surface is attributed to ordering in the charge sector with precisely the same wave vector as the one observed in STM and x rays [24,25]. (There is no ordering in the spin sector.) Signatures of charge order have also been seen in magnetic fields above 17 T in sound propagation experiments [9].

Recent nuclear magnetic resonance (NMR) experiments on the cuprate YBCO inside the (hole) doping region $0.11 < p < 0.12$ for the vortex state showed a charge modulation in the core of the vortices [26]. On the other hand, the authors of Ref. [7] studied YBCO in a magnetic field at hole doping $p = 0.12$ using the high-energy x-ray-scattering technique. They found the charge order not only in the pseudogap phase below an ordering temperature $T_{CDW} < T^*$, but also in the superconducting state with the maximum magnitude of the charge density wave (CDW) at the superconducting transition temperature T_c. Remarkably, below T_c the lattice modulation peak intensity grows linearly as a function of the magnetic field.

We can conclude from all these experiments that a charge-order state competes with the superconducting state in high-T_c cuprates and appears or is enhanced by a moderate magnetic field destroying or suppressing the superconductivity.

Recently, several of us have suggested to describe this competition between d-wave superconductivity and charge order in terms of a two-dimensional $O(4) \times O(4)$ symmetric nonlinear σ-model [27]. The components of the unit vectors represent fluctuating order parameters for superconductivity and a charge-modulated state. In this theory, the PG state is a fluctuating composite state made of superconducting and charge suborders corresponding to the disordered phase of the σ-model. The magnetic field can naturally be taken into account within this σ-model, and the competition between superconductivity and charge order can be explained and described using a renormalization-group scheme [28]. The results obtained in such a study are in good agreement with the results of the experiment on sound propagation [9].

The σ-model approach of Refs. [27,28] was further developed by Hayward *et al.* [29,30], who studied an O(6) symmetric σ-model that is identical to the $O(4) \times O(4)$ model if the superconducting phases of the two O(4) sectors are interlocked. Comparing the results of a Monte Carlo simulation based on this σ-model with experimental data on x-ray scattering, they reproduced the observed temperature dependency of the charge-order signal.

The nonlinear σ-model of Ref. [27] has been derived starting from the so-called spin-fermion model [31,32]. The charge order produced by this approach has been identified as

 ©2014 American Physical Society

a quadrupole density wave (QDW) with modulation vectors directed along the diagonals of the CuO lattice. The instability toward the charge modulation with this symmetry had been discussed earlier [33] under the name "valence bond solid." However, the fact that experiments so far see a primary charge order along the CuO bonds has been troubling theoreticians for years.

The CDW order with the modulation vectors directed along the bonds has been addressed by us in another publication [34] followed by several other proposals [35–38]. In Ref. [34], the CDW order is considered as a corollary attribute of the QDW/SC order, coexisting with it in the PG phase for $T < T_{\mathrm{CDW}}$ or in a strong magnetic field inside the superconducting phase. The CDW is only a byproduct of the SC/QDW order, induced by superconducting fluctuations, so that the shape of the transition lines in the T-B phase diagram, or the structure of the vortices, is determined by the competition between the SC and QDW suborders inside the PG phase.

Due to its unusual structure, it is not easy to observe the QDW order directly using nonresonant x-ray scattering. At the same time, the x-ray scattering may get a weaker signal from the secondary CDW order, and one can speak of studying the SC/QDW competition using the x-ray technique. For a σ-model description of the competition between SC and the experimentally observed CDW, x-ray scattering would probe this competition directly.

In this work, we use the nonlinear σ-model [27] to investigate the structure of a quantum vortex in the superconducting phase of a high-T_c superconductor. Previous works concentrated on general properties of the phase diagram without magnetic fields [27,34] or the transition from a uniform superconducting state into a uniform charge-ordered state under the influence of a strong magnetic field [28]. The properties of the vortex phase itself have remained an open question and are addressed by this work. We do not try to clarify the nature of the charge order here, assuming that it can be probed by different methods including x-ray scattering and STM spectroscopy.

For this purpose, we use the generalization of the nonlinear σ-model with a magnetic field introduced in Ref. [28]. Based on this model, we derive equations for the order parameter describing a quantum vortex carrying one magnetic flux quantum. We show that the symmetry of this order parameter leads to charge ordering inside the vortex core.

In a second step, we argue that this order is visible in x-ray scattering experiments by contributing to satellite peaks close to the standard Bragg peaks. Finally, the position of this satellite allows us to distinguish between the different types of charge-ordered states, QDW or CDW. We show that the modulation peak intensity should be proportional to the magnetic field, which is in agreement with the results of the experiment [7].

II. COMPOSITE ORDER PARAMETER AND MAIN EQUATIONS

A. Nonlinear σ-model

Below a temperature T^*, the spin-fermion model features a PG phase [27] characterized by an order parameter comprising both d-wave superconductivity and a charge order. Although the direct derivation leads to superconductivity competing with the QDW, the final equations can phenomenologically also be used for other types of charge order. As discussed in the Introduction, an additional charge order may be bound to the QDW, which allows one to observe the latter indirectly by, e.g., an x-ray technique. Thus, we consider explicitly the model with the SC/QDW composite order parameter as in Refs. [27,28] but having in mind also some broader applications, when discussing the symmetry of the charge order.

The order parameter may be represented in the form of an SU(2) unitary matrix in the particle-hole (Gorkov-Nambu) space,

$$u^L = \begin{pmatrix} \Delta^L_{\mathrm{QDW}} & \Delta^L_{\mathrm{SC}} \\ -\Delta^{L*}_{\mathrm{SC}} & \Delta^{L*}_{\mathrm{QDW}} \end{pmatrix}. \tag{1}$$

By unitarity, the parameters for the superconducting and charge orders, Δ^L_{SC} and Δ^L_{QDW}, are subject to the nonlinear constraint $|\Delta^L_{\mathrm{QDW}}|^2 + |\Delta^L_{\mathrm{SC}}|^2 = 1$. It is ultimately this constraint that leads to rather unusual superconducting properties of the system. The upper index $L = 1,2$ in Eq. (1) refers to the two quartets of hotspots, connected within the Brillouin zone by either $\mathbf{Q} = (\pi,\pi)$ for $L = 1$ or $(-\pi,\pi)$ for $L = 2$; see Fig. 1(a). In the hotspot-only approximation [27,33], these two quartets and their order parameters are decoupled.

Superconductivity and charge order are degenerate suborders of the pseudogap order described by Eq. (1). Finite curvature of the Fermi surface or a magnetic field lift the degeneracy below a temperature T_c, the former to favor superconductivity and the latter to support the charge order.

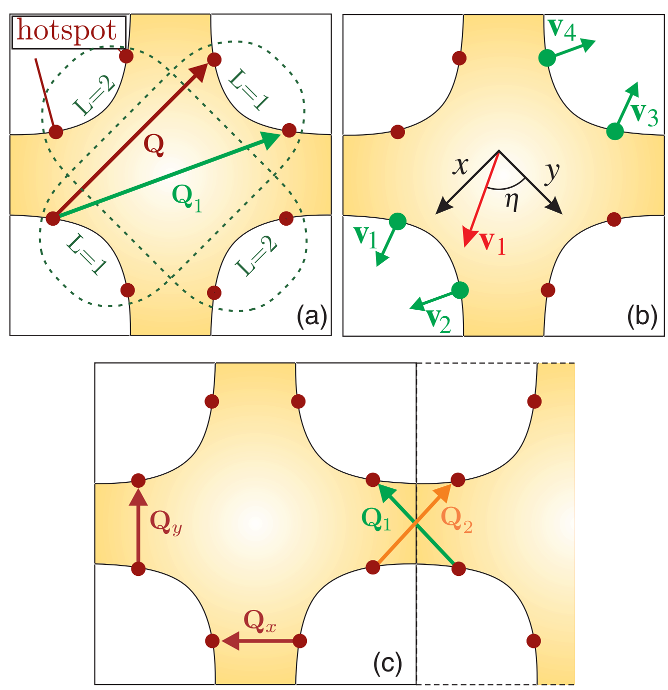

FIG. 1. (Color online) (a) Brillouin zone and hotspots connected with the antiferromagnetic wave vector $\mathbf{Q}$. Hotspots can be organized in terms of two quartets $L = 1$ and 2. (b) The hotspots forming the $L = 1$ quartet are indicated, and the velocities are defined via the angle η. (c) Wave vectors of the different orderings are presented. QDW order is modulated with $\mathbf{Q}_{1,2}$ while the CDW is modulated with $\mathbf{Q}_{x,y}$.

At higher temperatures, $T_c < T < T^*$, thermal fluctuations eventually restore the degeneracy. As these thermal fluctuations play a central role in our study, let us briefly discuss the nonlinear σ-model describing them. For an extensive discussion and derivation, we refer the reader to Ref. [27].

We are interested in the limit of long-wavelength thermal fluctuations, described by $u^L_{\mathbf{q}} = u^L_0 + \delta u^L_{\mathbf{q}}$ on small momenta $\mathbf{q}$. The fluctuation modes arise from coupling to the electrons; see Fig. 1(b). Let us consider the order parameter $u^{L=1}$, Eq. (1), for the first quartet. The order parameter $u^{L=1}$ coherently couples both hotspot 1 with 3 and hotspot 2 with 4. These pairs of hotspots are effectively nested, i.e., $\mathbf{v}_1 = -\mathbf{v}_3$ and $\mathbf{v}_2 = -\mathbf{v}_4$. As a result, the contribution to fluctuation modes due to the first pair of hotspots allows a momentum dependence only in the form of $(\mathbf{v}_1\mathbf{q})^2$, whereas the second pair leads to a dependence only on $(\mathbf{v}_2\mathbf{q})^2$. Being gapless, the fluctuation modes are thus described in the leading order by the free-energy functional $F_{L=1} = T\mathcal{F}_{L=1}$ with

$$\mathcal{F}_1[\delta u^1] = \frac{1}{2tv^2}\int \frac{d^2\mathbf{q}}{(2\pi)^2}\{(\mathbf{v}_1\mathbf{q})^2 + (\mathbf{v}_2\mathbf{q})^2\}\mathrm{tr}\big[\big(\delta u^1_q\big)^\dagger \delta u^1_q\big]. \tag{2}$$

The dimensionless coupling constant t is given by the temperature in units of the pseudogap scale T^*, $t = \alpha T/T^*$, with the numerical coefficient $\alpha \approx 0.74$ [27]. Choosing the coordinate axes along the diagonals of the Brillouin zone, see Fig. 1(b), we have $\mathbf{v}_1 = v(\sin\eta, \cos\eta)$ and $\mathbf{v}_2 = v(\sin\eta, -\cos\eta)$, with v the value of the Fermi velocity. Thus, $(\mathbf{v}_1\mathbf{q})^2 + (\mathbf{v}_2\mathbf{q})^2 = 2q_x^2\sin^2\eta + 2q_y^2\cos^2\eta$. Transforming to real space, we write the functional $\mathcal{F} = \mathcal{F}_1 + \mathcal{F}_2$ for the free energy of both quartets in the form of two σ-models on the manifold SU(2),

$$\mathcal{F}[u] = \frac{1}{t}\sum_{L=1}^{2}\int d^2\mathbf{r}\ \mathrm{tr}[\nabla^L(u^L)^\dagger\nabla^L u^L]. \tag{3}$$

For $\eta \neq 45^\circ$, the gradients ∇^L are anisotropic. For $L = 1$, we find according to our above analysis

$$\nabla^{L=1} = (\sin\eta\ \partial_x, \cos\eta\ \partial_y) \equiv \Gamma_1\nabla, \tag{4}$$

where

$$\Gamma_1 = \begin{pmatrix} \sin\eta & 0 \\ 0 & \cos\eta \end{pmatrix}. \tag{5}$$

For the quartet $L = 2$, obtained by turning the $L = 1$ quartet by 90°, the gradient reads

$$\nabla^{L=2} = (\cos\eta\ \partial_x, \sin\eta\ \partial_y) \equiv \Gamma_2\nabla, \tag{6}$$

with

$$\Gamma_2 = \begin{pmatrix} \cos\eta & 0 \\ 0 & \sin\eta \end{pmatrix}. \tag{7}$$

The different anisotropies in the two L sectors lead to unusual effects in the geometry of vortices in the presence of a magnetic field, as we will show below.

The σ-model (3) for the gapless fluctuations of the pseudogap order parameter has been derived for linear Fermi surfaces around the hotspots. Taking into account the finite curvature of the Fermi surface, we have to supplement the model (3) by the term [27]

$$\mathcal{F}_{\mathrm{curv}}[u] = \frac{\mu^2}{t}\sum_{L=1}^{2}\int d^2\mathbf{r}\ \mathrm{tr}[\tau_3(u^L)^\dagger\tau_3 u^L]. \tag{8}$$

The coupling constant μ has dimension of inverse length and grows with increasing the curvature. With τ_3 denoting the Pauli matrix in particle-hole space, we see that $\mathcal{F}_{\mathrm{curv}}$ breaks the symmetry between superconductivity and charge order favoring the superconducting suborder.

B. Vortex solution

Let us parametrize the unitary matrix u^L for the order parameter in Eq. (1) using polar coordinates. Introducing an "angle" θ^L between superconductivity and charge order, we write

$$\Delta^L_{\mathrm{QDW}} = \sin\theta^L e^{i\chi_L} \quad \text{and} \quad \Delta^L_{\mathrm{SC}} = \cos\theta^L e^{i\phi_L}. \tag{9}$$

The parameters χ_L and ϕ_L are the phases of the charge and superconducting order, respectively. Fluctuations of the phase χ_L of the charge order are relevant close to T_c but negligible in the regime $T \ll T_c$ in which we are interested. We therefore assume that $\chi_L = 0$ for both $L = 1$ and 2.

We include the magnetic field in the free-energy functional (3) by minimal coupling [28],

$$\nabla^L u^L \to \nabla^L u^L + \frac{ie}{c}\mathbf{A}^L[\tau_3, u^L],$$

where $\mathbf{A}^{L=1} = (\sin\eta\quad A_x, \cos\eta\quad A_y)$ and $\mathbf{A}^{L=2} = (\cos\eta\quad A_x, \sin\eta\quad A_y)$ are the reduced vector potentials due to the anisotropies in the two L-sectors. Furthermore, we add the contribution of the magnetic field to the free energy in units of temperature,

$$\mathcal{F}_B[\mathbf{A}] = \frac{1}{T}\int d^3\mathbf{r}\ \frac{[\nabla\times\mathbf{A}]^2}{8\pi}, \tag{10}$$

where $\mathbf{A} = (A_x, A_y, 0)$.

The σ-model has been derived for a single plane of CuO, and the total free energy is obtained by summing the contributions of all individual layers leading to an anisotropic three-dimensional (3D) model. Basically, two kinds of models are commonly used for the description of layered superconductors. For highly anisotropic systems, *discrete* two-dimensional layers are coupled by Josephson terms giving rise to interesting behavior of the vortex solution [39]. If the anisotropy is not very large, a continuous anisotropic 3D model is applicable. Actually, for fields perpendicular to the layers, the difference between these two model is not very important, and under the assumption that the magnetic field varies on length scales much larger than the layer thickness d, integration in the vertical z-direction simply yields a factor of d for each individual layer.

In the parametrization (9) of the order parameter, the σ-model (3) in the presence of the magnetic field reads

$$\mathcal{F}[\theta,\phi,\mathbf{A}] = \frac{2}{t}\sum_{L=1}^{2}\int d^2\mathbf{r}\Big\{(\nabla^L\theta^L)^2 + \Big(\nabla^L\phi_L + \frac{2e}{c}\mathbf{A}^L\Big)^2 \times \cos^2\theta^L - \mu^2\cos 2\theta^L\Big\}. \tag{11}$$

For each sector L, this model is reminiscent of the anisotropic Ginzburg-Landau functional [39]. However, the nonlinearity of the model (3) becomes noticeable in the cos-dependencies of the field θ^L. Also note that there are two order parameters θ^1 and θ^2, which in the presence of the magnetic field are coupled. The free-energy functional (11) is minimal for θ^L and $\mathbf{A}$ satisfying the Ginzburg-Landau-type equations

$$\nabla^L\nabla^L\theta^L + \frac{1}{2}\left(\nabla^L\phi_L + \frac{2e}{c}\mathbf{A}^L\right)^2 \sin 2\theta^L - \mu^2 \sin 2\theta^L = 0, \tag{12}$$

$$(\nabla\times\nabla\times\mathbf{A}) + \frac{32\pi e T^*}{c\alpha d}\sum_{L=1}^{2}\Gamma_L\left(\nabla^L\phi_L + \frac{2e}{c}\mathbf{A}^L\right) \times \cos^2\theta^L = 0, \tag{13}$$

with the "anisotropy matrices" Γ_L defined in Eqs. (5) and (7).

In the following, we are investigating the vortex solution for $\theta_L(\mathbf{r})$, associated with a magnetic flux equal to the flux quantum $\Phi_0 = \pi c/e$ [40]. For convenience, we choose the center of the vortex to be the origin. The anisotropy then suggests for the phases the spatial dependencies

$$\phi_{L=1} = \arctan\left(\tan\eta\,\frac{y}{x}\right)$$

and

$$\phi_{L=2} = \arctan\left(\cot\eta\,\frac{y}{x}\right).$$

The different anisotropic behavior for each L sector complicates the search for an exact solution of Eqs. (12) and (13). However, a simplification is possible because the superconducting order parameter and the magnetic field vary on different length scales. Indeed, θ_L becomes constant for $r = |\mathbf{r}| > \xi_{\mathrm{cor}}$ (with ξ_{cor} denoting the correlation length), whereas the magnetic field varies on the scale of the penetration depth λ, which for a strongly type-II superconductor is much larger. We will verify the validity of this assumption *a posteriori* by giving an estimate of the Ginzburg-Landau parameter $\kappa \equiv \lambda/\xi_{\mathrm{cor}}$ based on our analysis. Thus, as the first step, we determine the magnetic field using the fact that far from the vortex core, $\cos\theta^L \simeq 1$; cf. Eq. (9). Taking the curl on both sides of Eq. (13), we find that on scales $\gg \xi$,

$$\Delta\mathbf{B} - \lambda^{-2}\mathbf{B} = -\lambda^{-2}\Phi_0\delta(\mathbf{r})\mathbf{e}_z. \tag{14}$$

In terms of the microscopic parameters, the penetration depth λ is given by $\lambda^{-2} = 64\pi e^2 T^*/c^2 d\alpha$. Symmetry, in particular the absence of anisotropy, suggests using polar coordinates (r,φ). For the vector potential, we choose a gauge such that $\mathbf{A} = A(r)\mathbf{e}_\varphi$ and $d(rA)/dr = rB$ for $\mathbf{B}(r) = B(r)\mathbf{e}_z$. Proper boundary conditions are $A(0) = 0$ and $A(r) = \Phi_0/(2\pi r)$ for $r \to \infty$, guaranteeing a total magnetic flux of one flux quantum Φ_0.

With the magnetic field $\mathbf{B}(\mathbf{r})$ at hand, we are then in the position to determine the angular fields $\theta^L(\mathbf{r})$ using Eq. (12). For both quartets of hotspots, $L = 1$ and 2, we impose the same boundary conditions $\theta^L(0) = \pi/2$ and $\theta^L(\infty) = 0$, in line with the inherent d-wave symmetry of the order. It is convenient to perform for each sector L the coordinate transformation $\mathbf{r} = \Gamma_L\tilde{\mathbf{r}}$ with Γ_L defined in Eqs. (5) and (7). As a result, we have thus mapped the system of two anisotropic systems to two isotropic ones in L-dependent coordinates $\tilde{\mathbf{r}}$.

In spherical coordinates $(\bar{r},\varphi)$, where the dimensionless coordinate $\bar{r} = |\tilde{\mathbf{r}}|/\xi$ is the radius in units of the characteristic length $\xi = 1/(\sqrt{2}\mu)$, Eq. (12) is for each L reduced to

$$\Delta\theta_L + \frac{1}{2}\left(\frac{1}{\bar{r}} + \frac{e\sin(2\eta)\xi^2}{2c}B(0)\bar{r}\right)^2 \sin 2\theta_L - \frac{1}{2}\sin 2\theta_L = 0. \tag{15}$$

Deriving Eq. (15), we approximated the vector potential as $A(r) \simeq B(0)r/2$, which within the scale of the vortex constitutes the leading order. The second term in the large parentheses is parametrically much smaller than the first one [because $(e/c)\xi^2 B(0) = \kappa^{-2}\ln\kappa \ll 1$ [40]], and it may therefore be omitted in the numerical solution.

Vortex solutions to Eq. (15) are rotationally symmetric in the $\tilde{\mathbf{r}}$-coordinate system. Transforming back to the physical coordinates $\mathbf{r} = (x,y)$, we find for the hotspot quartet $L = 1$ that θ^1 depends on coordinates only as a function of $\sqrt{(x/\sin\eta)^2 + (y/\cos\eta)^2}$, while for the second quartet, $\theta^{L=2}$ is an effective function of $\sqrt{(x/\cos\eta)^2 + (y/\sin\eta)^2}$. Vortices in the superconducting order parameter have thus the shape of ellipses, with the ellipses in sectors $L = 1$ and 2 rotated by 90° with respect to each other.

III. VORTEX STATE

Generally, solving Eq. (15) requires numerical methods. Figure 2(a) shows among others a plot of $|\Delta_{\mathrm{SC}}| = \cos\theta^L$ as a function of the dimensionless radius $\bar{r}$. In certain limits, however, we may obtain approximate analytical solutions and use these solutions to estimate characteristic parameters of the system, such as the Ginzburg-Landau parameter κ. In the superconducting state, $\theta^L = 0$, while for $\theta^L = \pi/2$ the system shows pure charge order.

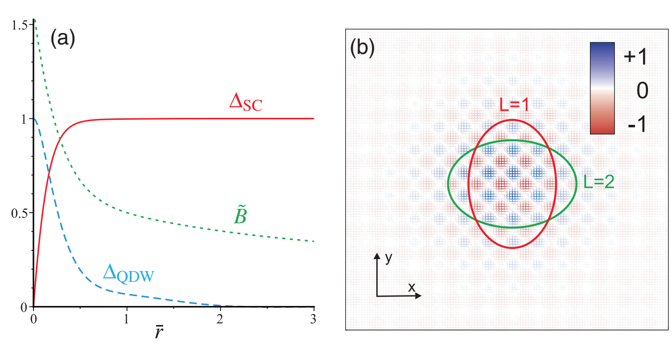

FIG. 2. (Color online) (a) Result of numerical studies of Eqs. (14) and (15) for a single vortex: superconducting order parameter Δ_{SC} (red, solid), charge order Δ_{QDW} (blue, dashed), and magnetic field $\tilde{B}$ (green, dotted) in arbitrary units as a function of the dimensionless radius $\bar{r}$. The nonlinear constraint on the total order parameter (1) leads to the rise of charge order triggered by simultaneous decay of the superconducting order. The magnetic field penetrates deep into the plane. (b) Checkerboard density wave order inside the vortex core of radius $\sim \xi$.

We assume that the system temperature is below T_c so that the system is a superconductor, which for a sufficiently strong magnetic field is penetrated by vortices. In the middle of the core of a single vortex, the superconducting order vanishes. Setting $\theta^L(\mathbf{r}) = \pi/2 + \delta\theta^L(\mathbf{r})$, we may then expand the left-hand side of Eq. (15) in $\delta\theta^L$. As a result, the problem is reduced to the single vortex in the conventional Ginzburg-Landau theory [40]. In particular, we find that the characteristic length parameter ξ determines the size of the vortex core and corresponds to the correlation length $\xi_{\rm cor}$. Thus, expressing the Ginzburg-Landau parameter κ in terms of the parameters of the model (11), we find the intermediate result

$$\kappa \sim \kappa^* \simeq \sqrt{\frac{\alpha c^2 d\mu^2}{32 e^2 \pi T^*}}. \tag{16}$$

The parameter μ^2 characterizing the curvature has been extracted [28] from the data for the zero-temperature critical magnetic field B_{c2} measured in a sound experiment on YBCO [9]. According to a fit in Ref. [28], $\mu^{-1} \approx 9$ nm. For the pseudogap temperature, we use $T^* \approx 250$ K and for the width d of a CuO layer the estimate $d \sim 10$ Å . Then, Eq. (16) yields the rough estimate of $\kappa^* \sim 10$ and already confirms the assumption of a rather strongly type-II superconductor used when making approximations.

However, a more accurate estimate shows that the correlation length $\xi_{\rm cor}$ is smaller than the characteristic length ξ in Eq. (15) so that κ becomes even larger. Indeed, based on the numerical solution for the nonlinear equation for $\Delta_{\rm SC}$, cf. Fig. 2(a), we extract an estimate for the correlation length as the length at which $\Delta_{\rm SC} = 1/2$. This procedure yields $\xi_{\rm cor} \approx 0.1\xi$. As a result of this refined analysis, we thus obtain a Ginzburg-Landau parameter

$$\kappa \approx 10\kappa^* \sim 100.$$

This still rough order-of-magnitude estimate is in line with the literature [39], although perhaps somewhat larger than expected. In particular, it *a posteriori* justifies the approximations done in Sec. II.

Let us now dwell on more nontrivial effects resulting from the nonlinear σ-model for matrices u^L, Eq. (1). We have already seen that the nonlinear constraint $|\Delta^L_{\rm QDW}|^2 + |\Delta^L_{\rm SC}|^2 = 1$ between the superconducting and charge suborders effectively enhances the inverse correlation length $\xi^{-1}_{\rm cor}$. More strikingly, this constraint makes charge order emerge automatically as soon as superconductivity is (locally) suppressed by the magnetic field [28]. As a result, the vortex cores carry charge order. Moreover, as shown in Fig. 2, there is a region around a vortex between the radius scales of $\xi_{\rm cor}$ and ξ where superconductivity coexists with still appreciable charge order.

In real space, as discussed in Sec. II, the vortices in each of the two sectors L for the two quartets of hotspots have in general elliptic shapes. Only for the special angle of $\eta = 45^\circ$, cf. Fig. 1, do these ellipses turn into circles that for both sectors are the same. In the general situation, $\eta \neq 45^\circ$ and the two sectors L feature anisotropic vortices that are rotated by 90° with respect to each other. As a result, while breaking rotational symmetry, the geometry of a single vortex reflects the d-wave spatial symmetry. Figure 2(b) visualizes the checkerboard charge order inside the two crossed vortices. At the boundaries, where due to the anisotropy only one of the L sectors still shows vortex features, the density shows a (very) local stripe structure.

IV. DISCUSSION OF X-RAY EXPERIMENTS

Let us now address the question of how the predicted state can be observed in x-ray experiments. By conventional hard-x-ray scattering techniques, one basically measures the Fourier transform of the charge density. A charge order is thus in principle detectable using such experiments. Below T_c, our theoretical analysis based on the σ-model for the pseudogap state shows the emergence of a charge order inside vortex cores, provided a sufficiently strong magnetic field creates vortices. This competing charge order has been identified in Ref. [27] as a quadrupole density wave, or equivalently bond order [33]. This order is characterized by two charge density wave orders on the Cu bonds, where the oxygen atoms are situated. A phase difference of π between O atoms on bonds in the x direction and those in the y direction established the quadrupolar charge order around each Cu atom.

Explicitly, the QDW leads to a charge modulation of oxygen atoms [27] of the form

$$\rho_{{\rm QDW},x/y}(\mathbf{r}) = \pm|\Delta_{\rm QDW}|[\sin(\mathbf{Q}_1\mathbf{r}) + \sin(\mathbf{Q}_2\mathbf{r})]. \tag{17}$$

The overall sign is different for bonds in the x and y directions. The wave vectors $\mathbf{Q}_1$ and $\mathbf{Q}_2$ connect opposing hotspots; see Fig. 1(c).

Since at each site in the Cu lattice the average charge density associated with the QDW modulation of formula (17) is zero, the QDW itself seems difficult to impossible to detect in x-ray experiments. Also, the wave vectors $\mathbf{Q}_1$ and $\mathbf{Q}_2$ are not the ones observed in either STM [26,41] or x -ray [21] experiments, which instead indicate wave vectors $\mathbf{Q}_x$ and $\mathbf{Q}_y$ along the bonds, cf. Fig. 1(c). At the same time, theoretical approaches that take a microscopic point of view, assuming for example a model of a single antiferromagnetic quantum critical point [27,33,42], typically identify the QDW with wave vectors $\mathbf{Q}_1$ and $\mathbf{Q}_2$ to be the order associated with the leading instability in the particle-hole channel. Very recently, theoretical ideas and mechanisms [34,36,37] have been developed that may supplement the QDW picture [33,34] by a true charge density wave order on the Cu atoms with the experimentally observed wave vectors. These ideas include extensions of the quantum critical hotspot model [34], taking into account strong on-site Coulomb interactions [36] and nontrivial interplay between charge order and superconducting fluctuations [34,36–38]. It is not yet clear, though, whether the CDW will eventually have to be regarded as coexisting or competing with the QDW. Taking a phenomenological approach [29,30], we choose in the following to discuss the simplest picture of a nonlinear σ-model with the CDW being the competitor of superconductivity instead of the QDW. In this case, we assume the following form of the charge density on the Cu atoms:

$$\rho_{\rm CDW}(\mathbf{r}) = |\Delta_{\rm CDW}|[\sin(\mathbf{Q}_x\mathbf{r}) + \sin(\mathbf{Q}_y\mathbf{r})] \tag{18}$$

with the observed wave vectors $\mathbf{Q}_x$ and $\mathbf{Q}_y$. As before, the CDW is assumed to appear as soon as the superconducting order decays due to vortex generation in sufficiently strong

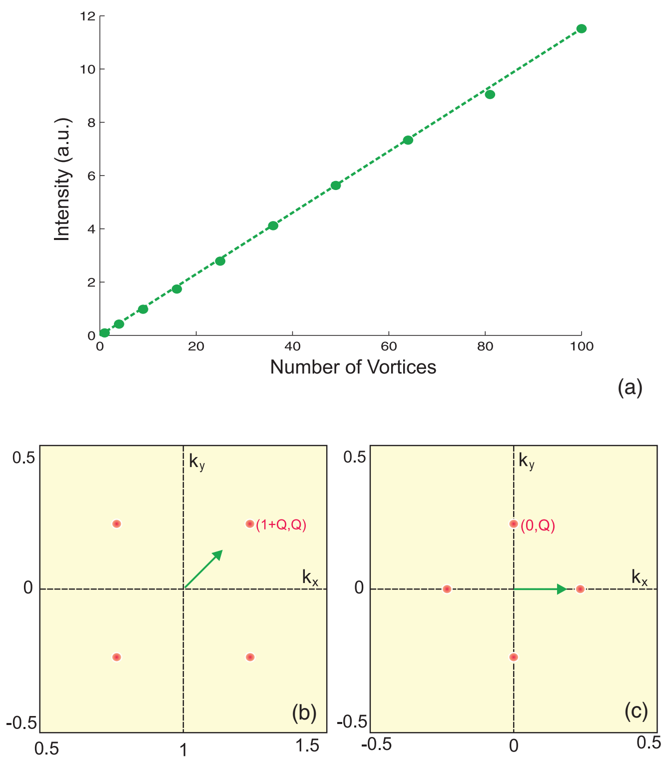

FIG. 3. (Color online) (a) Vortex contribution to the intensity of one (200) satellite peak. The linear behavior is clearly visible. (b),(c) Peak structure of the QDW and CDW order, respectively. The satellites to the (000) and (100) Bragg peaks are shown.

magnetic fields. The CDW at the vortex cores should be easily detectable in x-ray experiments.

To be specific, the x-ray-scattering intensity is determined by the density-density structure factor, which reads here

$$I_{\mathbf{q}} = \rho_{\mathbf{q}}\rho_{-\mathbf{q}} \tag{19}$$

with $\rho_{\mathbf{q}} = \sum_{\mathbf{r}} \exp(-i\mathbf{q}\cdot\mathbf{r})\rho(\mathbf{r})$ the Fourier transform of the charge density. Herein, the sum is over all lattice sites $\mathbf{r}$ in the CuO lattice, and $\rho(\mathbf{r})$ is equal to $\rho_{\mathrm{CDW}}(\mathbf{r})$, Eq. (18), if $\mathbf{r}$ is a Cu site, and given by $\rho_{\mathrm{CDW}}(\mathbf{r}) + \rho_{\mathrm{QDW},x/y}(\mathbf{r})$, cf. Eq. (17), if $\mathbf{r}$ is an oxygen site on a Cu bond in the x or y direction, respectively.

The structure factor (19) in the presence of the CDW and QDW charge orders specified by Eqs. (17) and (18) leads to satellites around the standard Bragg peaks as shown in Figs. 3(b) and 3(c). Within the σ-model theory for the pseudogap state, we expect these charge-order-related peak to appear both at very high magnetic fields $B > H_{c2}$ so that the system is in a pure charge order state, and with a lower intensity at intermediate fields $H_{c1} < B < H_{c2}$ where charge order exists inside the vortex cores. We note that the QDW only contributes to "odd" Bragg peaks, i.e., where the sum of the two integers n and m in the reciprocal-lattice vector $\mathbf{K} = (2\pi/a)(n,m)$ is odd. Since QDW order thus grants a signal only at the edge of the first Brillouin zone, its observation will probably be a challenge.

Finally, let us examine the regime above H_{c1} where many vortices appear and the vortices form a lattice. The calculation is straightforward; every vortex has a similar structure to the single vortex. The number of vortices must be proportional to the applied magnetic field $\mathbf{B}$, and we are interested in the evolution of the scattering intensity of a charge-order peak.

The numerical solution is obtained by calculation of the integrated intensity for a given number of vortices, which are well separated by using Eq. (19), and integration of this result over the wave vectors close to the peak. This procedure results in Fig. 3(a), revealing that the integrated intensity is proportional to the number of vortices, where the number of vortices is in turn proportional to the applied magnetic field. Thus, $I^{\mathrm{peak}}_{\mathbf{q}_0} \propto |\mathbf{B}|$. This result is in agreement with a recent experimental work [7].

The authors of this study performed a hard-x-ray experiment and found satellites to the (2 0 0.5) and (0 2 0.5) Bragg peaks that were interpreted as a result of the formation of CDW order in the CuO planes. At zero field, the charge order emerges by cooling the system below a critical temperature $T_{\mathrm{CDW}} \approx 150$ K.

The situation at zero field suggests that this charge signal is a consequence of the coexistence between superconductivity and charge density wave order. This is in line with our theoretical finding in Ref. [34] . On the other hand, the increase of the signal strength by applying the magnetic field can be attributed to the formation of vortices in the CuO plane. Outside the vortices, superconductivity suppresses the charge order and a field-independent signal is obtained. Inside the vortices, there are regions that are purely charge-ordered, further enhancing the signal. Increasing the magnetic field allows more vortices to penetrate the sample and thus leads to a stronger signal. This can be seen in Fig. 2(b) of Ref. [7]. Remarkably, the increase is a linear function of the applied magnetic field, as suggested.

Further evidence for charge order inside vortex cores was found in Refs. [18,26]. The authors of Ref. [26] found a charge-order signal by means of NMR measurement inside the superconducting phase when a magnetic field is applied. For fixed temperature, the order starts to give a signal above some threshold field H_{charge}. Whether the order is uni- or bidirectional was not specified and therefore it is not completely clear which kind of charge order emerges there, but the appearance of charge order in the vortex phase confirms our theoretical finding.

A similar scenario applies to Ref. [18], where charge order in the vortices was found in an STM experiment. It was verified that the order has checkerboard symmetry and therefore fits nicely into our theoretical findings.

V. CONCLUSION

The σ-model description [27] for the pseudogap in the high-T_c cuprates leads to vortices whose geometry may differ from the conventional Ginzburg-Landau picture. The main difference, however, is the onset of charge order in the vortex core, where the superconducting order parameter turns to zero. This gives rise to peaks in the density-density structure factor and explains the CDW signals seen in x-ray experiments [7,18,26]. We hope that future experimental works will soon clarify the theoretically troubling issue of charge-order x-ray peaks along the diagonal of the Brillouin zone.

ACKNOWLEDGMENTS

K.B.E. and M.E. gratefully acknowledge financial support from the Ministry of Education and Science of the Russian Federation in the framework of Increase Competitiveness Program of NUST "MISiS" (Nr. K2-2014-015). Financial support of K.B.E. and M.E. by SFB/TR12 of DFG is gratefully appreciated. H.M. acknowledges the Yale Prize Postdoctoral Fellowship and C.P. acknowledges the support PALM Labex grant Excelcius.

[1] J. G. Bednorz and K. A. Müller, Z. Physik B **64**, 189 (1986).
[2] W. D. Wise, M. C. Boyer, K. Chatterjee, T. Kondo, T. Takeuchi, H. Ikuta, Y. Wang, and E. W. Hudson, Nat. Phys. **4**, 696 (2008).
[3] M. J. Lawler, K. Fujita, J. Lee, A. R. Schmidt, Y. Kohsaka, C. K. Kim, H. Eisaki, S. Uchida, J. C. Davis, J. P. Sethna, and E.-A. Kim, Nature (London) **466**, 347 (2010).
[4] T. Wu, H. Mayaffre, S. Krämer, M. Horvatić, C. Berthier, W. N. Hardy, R. Liang, D. A. Bonn, and M.-H. Julien, Nature (London) **477**, 191 (2011).
[5] C. V. Parker, P. Aynajian, E. H. da Silva Neto, A. Pushp, S. Ono, J. Wen, Z. Xu, G. Gu, and A. Yazdani, Nature (London) **468**, 677 (2010).
[6] G. Ghiringhelli, M. Le Tacon, M. Minola, S. Blanco-Canosa, C. Mazzoli, N. B. Brookes, G. M. De Luca, A. Frano, D. G. Hawthorn, F. He, T. Loew, M. Moretti Sala, D. C. Peets, M. Salluzzo, E. Schierle, R. Sutarto, G. A. Sawatzky, E. Weschke, B. Keimer, and L. Braicovich, Science **337**, 821 (2012).
[7] J. Chang, E. Blackburn, A. T. Holmes, N. B. Christensen, J. Larsen, J. Mesot, R. Liang, D. A. Bonn, W. N. Hardy, A. Watenphul, M. v. Zimmermann, E. M. Forgan, and S. M. Hayden, Nat. Phys. **8**, 871 (2012).
[8] A. J. Achkar, R. Sutarto, X. Mao, F. He, A. Frano, S. Blanco-Canosa, M. Le Tacon, G. Ghiringhelli, L. Braicovich, M. Minola, M. Moretti Sala, C. Mazzoli, R. Liang, D. A. Bonn, W. N. Hardy, B. Keimer, G. A. Sawatzky, and D. G. Hawthorn, Phys. Rev. Lett. **109**, 167001 (2012).
[9] D. LeBoeuf, S. Krämer, W. N. Hardy, R. Liang, D. A. Bonn, and C. Proust, Nat. Phys. **9**, 79 (2013).
[10] E. Blackburn, J. Chang, M. Hücker, A. T. Holmes, N. B. Christensen, R. Liang, D. A. Bonn, W. N. Hardy, U. Rütt, O. Gutowski, M. v. Zimmermann, E. M. Forgan, and S. M. Hayden, Phys. Rev. Lett. **110**, 137004 (2013).
[11] J. Zaanen and O. Gunnarsson, Phys. Rev. B **40**, 7391(R) (1989).
[12] K. Machida, Physica C **158**, 192 (1989).
[13] D. Poilblanc and T. M. Rice, Phys. Rev. B **39**, 9749 (1989).
[14] J. M. Tranquada, B. J. Sternlieb, J. D. Axe, Y. Nakamura, and S. Uchida, Nature (London) **375**, 561 (1995).
[15] V. J. Emery, S. A. Kivelson, and J. M. Tranquada, Proc. Natl. Acad. Sci. (USA) **96**, 8814 (1999).
[16] S. A. Kivelson, I. P. Bindloss, E. Fradkin, V. Oganesyan, J. M. Tranquada, A. Kapitulnik, and C. Howald, Rev. Mod. Phys. **75**, 1201 (2003).
[17] S. R. White and D. J. Scalapino, Phys. Rev. Lett. **80**, 1272 (1998).
[18] J. E. Hoffman, E. W. Hudson, K. M. Lang, V. Madhavan, H. Eisaki, S. Uchida, and J. C. Davis, Science **295**, 466 (2002).
[19] G. Levy, M. Kugler, A. A. Manuel, Ø. Fischer, and M. Li, Phys. Rev. Lett. **95**, 257005 (2005).
[20] K. Matsuba, S. Yoshizawa, Y. Mochizuki, T. Mochiku, K. Hirata, and N. Nishida, J. Phys. Soc. Jpn. **76**, 063704 (2007).
[21] R. Comin, R. Sutarto, F. He, E. da Silva Neto, L. Chauviere, A. Frano, R. Liang, W. N. Hardy, D. Bonn, Y. Yoshida, H. Eisaki, J. E. Hoffman, B. Keimer, G. A. Sawatzky, and A. Damascelli, arXiv:1402.5415.
[22] N. Doiron-Leyraud, C. Proust, D. LeBoeuf, J. Levallois, J. Bonnemaison, R. Liang, D. A. Bonn, W. N. Hardy, and L. Taillefer, Nature (London) **447**, 565 (2007).
[23] F. Laliberté, J. Chang, N. Doiron-Leyraud, E. Hassinger, R. Daou, M. Rondeau, B. J. Ramshaw, R. Liang, D. A. Bonn, W. N. Hardy, S. Pyon, T. Takayama, H. Takagi, I. Sheikin, L. Malone, C. Proust, K. Behnia, and L. Taillefer, Nat. Commun. **2**, 432 (2011).
[24] S. E. Sebastian, N. Harrison, R. Liang, D. A. Bonn, W. N. Hardy, C. H. Mielke, and G. G. Lonzarich, Phys. Rev. Lett. **108**, 196403 (2012).
[25] S. E. Sebastian, N. Harrison, and G. G. Lonzarich, Rep. Prog. Phys. **75**, 102501 (2012).
[26] T. Wu, H. Mayaffre, S. Krämer, M. Horvatic, C. Berthier, P. L. Kuhns, A. P. Reyes, R. Liang, W. N. Hardy, D. A. Bonn, and M. H. Julien, Nat. Commun. **4**, 2113 (2013).
[27] K. B. Efetov, H. Meier, and C. Pépin, Nat. Phys. **9**, 442 (2013).
[28] H. Meier, M. Einenkel, C. Pépin, and K. B. Efetov, Phys. Rev. B **88**, 020506(R) (2013).
[29] L. E. Hayward, D. G. Hawthorn, R. G. Melko, and S. Sachdev, Science **343**, 1336 (2014).
[30] L. E. Hayward, A. J. Achkar, D. G. Hawthorn, R. G. Melko, and S. Sachdev, arXiv:1406.2694.
[31] Ar. Abanov and A. V. Chubukov, Phys. Rev. Lett. **84**, 5608 (2000).
[32] Ar. Abanov, A. V. Chubukov, and J. Schmalian, Adv. Phys. **52**, 119 (2003).
[33] M. A. Metlitski and S. Sachdev, Phys. Rev. B **82**, 075128 (2010).
[34] H. Meier, C. Pepin, M. Einenkel, and K. B. Efetov, Phys. Rev. B **89**, 195115 (2014).
[35] Y. Wang and A. V. Chubukov, arXiv:1401.0712.
[36] A. Allais, J. Bauer, and S. Sachdev, arXiv:1402.4807; Ind. J. Phys. 0973-1458 (2014).
[37] D. Chowdhury and S. Sachdev, arXiv:1404.6532.
[38] A. Allais, D. Chowdhury, and S. Sachdev, arXiv:1406.0503.
[39] G. Blatter, M. V. Feigel'man, V. B. Geshkenbein, A. I. Larkin, and V. M. Vinokur, Rev. Mod. Phys. **66**, 1125 (1994).
[40] M. Tinkham, *Introduction to Superconductivity* (McGraw-Hill, New York, 1975).
[41] R. Comin, A. Frano, M. M. Yee, Y. Yoshida, H. Eisaki, E. Schierle, E. Weschke, R. Sutarto, F. He, A. Soumyanarayanan, Y. He, M. Le Tacon, I. S. Elfimov, J. E. Hoffman, G. A. Sawatzky, B. Keimer, and A. Damascelli, Science **343**, 390 (2013).
[42] S. Sachdev and R. La Placa, Phys. Rev. Lett. **111**, 027202 (2013).